ChemComm

COMMUNICATION

View Article Online
View Journal | View Issue

Cite this: *Chem. Commun.*, 2021, **57**, 8174

Received 18th June 2021,
Accepted 16th July 2021

DOI: 10.1039/d1cc03232a

rsc.li/chemcomm

Sensitive imaging of tumors using a nitroreductase-activated fluorescence probe in the NIR-II window†

Xiaofan Zhang,[ab] Xiaohua Li,[*ab] Wen Shi[ab] and Huimin Ma[*ab]

A nitroreductase (NTR)-activated NIR-II fluorescence probe for tumor imaging is reported. The probe can emit fluorescence in the range of 900–1300 nm, and target hypoxic tumors with NTR overexpression, thus allowing for accurate delineation of tumor margins through deep penetration.

Surgical resection of tumors is an effective method for treatment of cancer in clinical surgical oncology.[1] However, the accurate delineation of tumor margins remains a challenge. Among the methods employed, fluorescence imaging has become a promising way due to its real-time, convenient and noninvasive optical visualization with high sensitivity.[2] Particularly, fluorescence imaging in the second near-infrared window (NIR-II, 1000–1700 nm) exhibits reduced photon scattering and absorption as well as negligible background auto-fluorescence in living tissues, thus leading to deeper penetration and higher spatio-temporal resolution.[3]

For some tumor tissues and cells, such as 4T1 and A549, one of the most common features is hypoxia. The hypoxic microenvironment endows cancer cells with higher resistance towards cancer chemotherapy and radiotherapy.[4] Therefore, it is of great clinical significance to evaluate the hypoxic degree in tumors, which is known to be directly associated with the expression of nitroreductase (NTR), a tumor marker.[5] So far, many small molecular fluorescent probes have been reported for NTR detection. However, most of them emit in the traditional visible and NIR-I (650–900 nm) spectral region, which may suffer from limited imaging depth.[6] For hypoxic NTR detection and *in vivo* imaging of tumors, fluorescence probes which not only possess longer emission wavelengths (beyond 900 nm, better extended to the NIR-II region) but also give off–on fluorescence responses are more desirable because they produce light signals only after the specific interaction with the tumor marker and show lower background noise and clearer discrimination between the tumor and the surrounding normal tissue.[7] Although significant effort has been made for this purpose,[8] the sensitivity of most existing NTR fluorescent probes that emit beyond 900 nm is still inadequate for detecting trace levels of NTR in common biosystems. Thus, it is highly demanded to develop sensitive fluorescence off–on probes with the emission extended to the NIR-II region for accurate delineation of tumor margins. In fact, high sensitivity has always been one of the most important scientific issues and research topics (including high selectivity and simple, inexpensive practicality) in the field of spectroscopic probes.[9]

Herein, a new fluorescence off–on probe (RHC-NO_2) for NTR is presented (Scheme 1) that is suitable for fluorescence imaging in the NIR-II window. It provides a much lower detection limit (5.9 ng mL^{-1}) than the other current NTR-activated NIR-II probes.[10] Probe RHC-NO_2, with an emission peak at 921 nm, was designed by using the rhodamine hydrid polymethine framework. Meanwhile, a nitro group, serving as the NTR-specific recognition moiety as well as the fluorescence quencher, was incorporated into the skeleton. Upon reaction of the probe with NTR, the nitro group was reduced to an amino group and the fluorescence at 921 nm was recovered accordingly (Scheme 1). The fluorescence off–on response provided a largely reduced background noise, thus leading to a high signal-to-background ratio in intravital imaging. Using this probe, fluorescence imaging of tumors was successfully

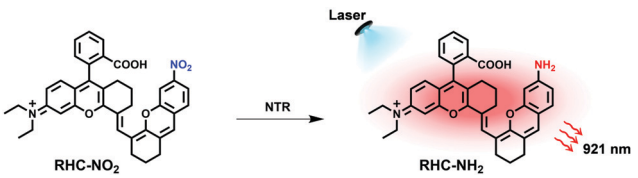

Scheme 1 Sensing mechanism of RHC-NO_2 for NTR detection.

[a] *Beijing National Laboratory for Molecular Sciences, Key Laboratory of Analytical Chemistry for Living Biosystems, Institute of Chemistry, Chinese Academy of Sciences, Beijing 100190, China. E-mail: lixh@iccas.ac.cn, mahm@iccas.ac.cn*
[b] *University of Chinese Academy of Sciences, Beijing 100049, China*

† Electronic supplementary information (ESI) available. See DOI: 10.1039/d1cc03232a

achieved in two kinds of murine tumor models (A549 and HeLa tumors).

The absorption spectra of the probe with and without NTR were studied in pH 7.4 phosphate buffer (PBS). As shown in Fig. 1A, probe RHC-NO_2 exhibits a maximum absorption at 677 nm. Addition of NTR results in the emergence of a new absorption peak at 868 nm, which may be attributed to the formation of the reaction product, RHC-NH_2. The fluorescence emission spectra of RHC-NO_2 with and without NTR are depicted in Fig. 1B. It is seen that the probe itself is almost non-fluorescent (quantum yield $\Phi < 0.01\%$) due to the quenching effect of the nitro group, but the reaction with NTR produces strong fluorescence at 921 nm (about 14-fold enhancement). Meanwhile, the spectral properties of the synthesized RHC-NH_2 (reaction product) were examined. As expected, RHC-NH_2 also shows maximal absorption and fluorescence emission at 868 nm and 921 nm, respectively, in PBS of pH 7.4 (Fig. S10, ESI†). These results suggested the possible generation of RHC-NH_2 upon reaction of the probe with NTR.

To further prove this, the reaction products of RHC-NO_2 with NTR were subjected to ESI-MS and HPLC analysis (Fig. S11 and S12, ESI†), which indicated that the NTR-catalyzed reduction of the probe indeed produced RHC-NH_2. Moreover, the stability of RHC-NO_2 was investigated by measuring its absorption and fluorescence spectra in PBS for different periods of time (Fig. S13, ESI†). The results showed that the probe was rather stable at room temperature, which was favourable for *in vivo* imaging.

In addition, the fluorescence intensity of RHC-NO_2 and RHC-NH_2 was compared in pH 7.4 phosphate buffer containing different fractions of FBS (Fig. S14, ESI†). It was found that the probe itself exhibited very weak fluorescence either with FBS or without FBS, whereas RHC-NH_2 displayed a largely enhanced fluorescence with increasing the fraction of FBS in PBS, which may arise from the possible formation of the dye-protein complex.[11] Thus, in the following experiments, the reactions of RHC-NO_2 with NTR were studied in the phosphate buffer (20 mM, pH 7.4) containing 10% volume fraction of FBS, which may be used to simulate the physiological environment.[12]

The influence of NADH (a cofactor of NTR) on the fluorescence response was investigated, and 200 μM of NADH was found to achieve the maximal fluorescence signal (Fig. S15, ESI†), which was roughly matchable to the basal level (about 30–168 μM)[13] of NADH in common biosystems. Moreover, the reaction conditions (such as time, pH and temperature) were also optimized. The time-dependent fluorescence response of the probe toward NTR is shown in Fig. S16 (ESI†), from which it can be seen that the fluorescence intensity increases rapidly at 921 nm and reaches a plateau in about 1 h. Meanwhile, pH and temperature fluctuations hardly affected the fluorescence of RHC-NO_2, and the reaction of the probe with NTR proceeded well at pH 7.4 and 37 °C (Fig. S17, ESI†), demonstrating its outstanding biological applicability under the physiological conditions.

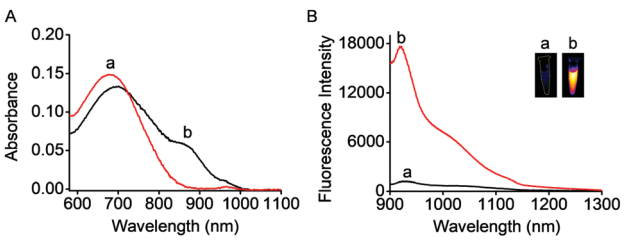

Fig. 1 (A) Absorption and (B) fluorescence spectra of RHC-NO_2 (10 μM) before (a) and after (b) reaction with NTR (10 μg mL^{-1}) in the presence of NADH (200 μM) in pH 7.4 phosphate buffer containing 10% fetal bovine serum (FBS). Inset: NIR-II fluorescence images of RHC-NO_2 in test tubes before (a) and after (b) reaction with NTR, with an exposure time of 50 ms (excited with 808 nm laser) and 1000 nm long-pass emission filter.

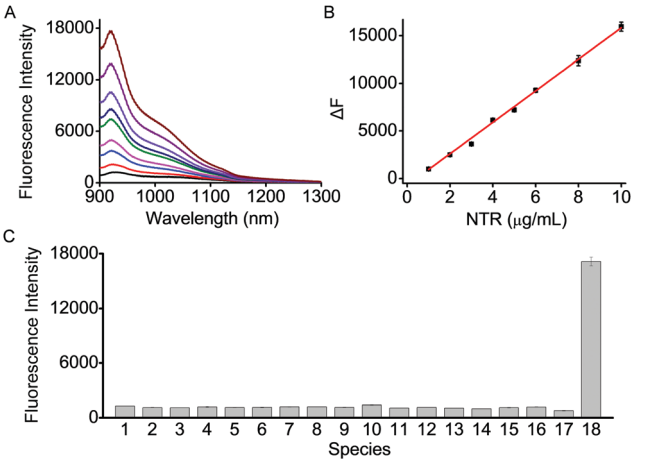

Fig. 2 (A) Fluorescence response of RHC-NO_2 (10 μM) to varied concentrations of NTR (0–10 μg mL^{-1}). (B) Linear fitting curve of ΔF against the concentration of NTR. (C) Fluorescence response of RHC-NO_2 to various species (from 1 to 18): blank, cysteine (1 mM), glutathione (1 mM), Na_2S (100 μM), vitamin C (1 mM), H_2O_2 (100 μM), NaOCl (100 μM), $NaNO_2$ (100 μM), •OH (100 μM), Ca^{2+} (2 mM), Cu^{2+} (100 μM), Fe^{2+} (100 μM), glucose (10 mM), K^+ (150 mM), Mg^{2+} (2 mM), Zn^{2+} (100 μM), $ONOO^-$ (200 μM), NTR (10 μg mL^{-1}). The results are the mean ± standard deviation of three separate measurements.

Under the optimized conditions (reaction at 37 °C for 1 h in PBS of pH 7.4 containing 10% FBS in the presence of 200 μM NADH), the fluorescence response of RHC-NO_2 to NTR at varied concentrations is shown in Fig. 2A and B, revealing that the fluorescence intensity at 921 nm gradually increases with increasing NTR. There is a good linearity between ΔF and the concentration of NTR in the range of 1–10 μg mL^{-1}, with an equation of $\Delta F = 1657 \times [C\ (\mu g\ mL^{-1})] - 730$ ($R = 0.994$) and a detection limit of as low as 5.9 ng mL^{-1}, where ΔF is the difference of fluorescence intensity of RHC-NO_2 with and without NTR at 921 nm. These observations suggested that RHC-NO_2 may be applied for *in vivo* imaging *via* the detection of trace concentrations of NTR in the NIR-II window.

In order to get an insight into the selectivity of the probe, fluorescence responses were tested in the presence of various potential interfering species. As shown in Fig. 2C, no significant fluorescence response is detected among the substances tested, including inorganic salts (Na_2S, $CaCl_2$, $CuSO_4$, $FeSO_4$, KCl, $MgCl_2$, $ZnCl_2$), vitamin C, glucose, reactive oxygen species

(H_2O_2, NaOCl, $NaNO_2$, $^{\bullet}OH$, $ONOO^-$) and biothiols (cysteine, glutathione). By contrast, the addition of NTR causes remarkable fluorescence increase, revealing that RHC-NO_2 exhibits high selectivity for NTR even in complex biological environment.

Next, enzyme inhibition experiments were performed to further verify that the fluorescence response was generated by the NTR-catalyzed reaction. As seen from Fig. S18 (ESI†), the fluorescence intensity with 0.1 mM dicoumarin (curve d) is much weaker than that (curve c) without the inhibitor, and more dicoumarin (0.2 mM) results in a greater decrease in fluorescence intensity (curve e). These results suggest that the fluorescence off–on response indeed arises from the enzyme catalyzed reaction.

Besides, the spectral properties of RHC-NH_2 were explored in different solvents (Fig. S19 and Table S1, ESI†), and similar spectral properties, *i.e.*, with the maximum absorption/emission at about 850/920 nm but an increased quantum yield up to about 0.1%, were observed, though the absorption or fluorescence intensities were affected by the variation of solvents. The pH effects on the spectral properties are displayed in Fig. S20 (ESI†), disclosing that the absorption at 868 nm hardly changes and strong NIR fluorescence beyond 900 nm is observed in a wide span of pH from 4 to 10, though the fluorescence becomes stronger in an alkaline medium. This suggests that RHC-NH_2, with bright emission in the NIR-II region, may act as a useful platform for designing activatable long wavelength fluorescent probes through further modification of its amino group.

The cytotoxicity of probe RHC-NO_2 was assessed by the standard MTT assay before its application for *in vivo* imaging (Fig. S21, ESI†), and no significant toxicity was observed in the case of A549 or HeLa cell line, suggesting the good biocompatibility of the probe.

Bearing in mind that the probe displayed the merits of bright fluorescence beyond 900 nm, excellent stability and biocompatibility, we applied it to NIR-II fluorescence imaging of tumor in living animals. In this experiment, female BALB/c nude mice bearing the subcutaneous A549 tumor were chosen as a model because of the elevated level of NTR under hypoxic conditions. Probe RHC-NO_2 was intravenously injected into A549 tumor-bearing mice. As is seen from Fig. 3 and Fig. S22 (ESI†), the fluorescence intensity in the tumor gradually increases and the maximal NIR-II signal is detected after about 12 h of injection. Then, the fluorescence decreases with time. Most importantly, the tumor becomes distinguishable from the surrounding normal tissue after 4 h of injection, and the tumor boundary remains clear until about 24 h. As mentioned above, the fluorescence enhancement could be ascribed to the reaction of RHC-NO_2 with the overexpressed NTR in A549 tumors. It is noticed that upon injection of the probe, the fluorescence is also observed in other parts of the mouse body besides the tumor region, which is probably attributed to the metabolism of the probe *via* the liver and kidney (such metabolic pathways are quite common in previously reported literature[14]). Moreover, after 24 h of injection, the fluorescence in the tumor remains bright, while that in other organs becomes quite weak. Therefore, 24 h may be selected as the time point for

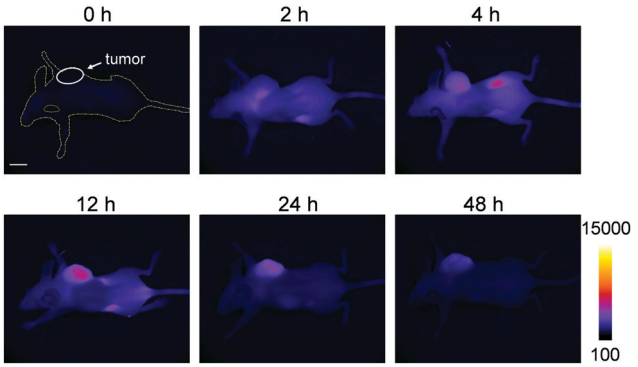

Fig. 3 Representative NIR-II images of A549 tumor-bearing mice (n = 3) after tail vein injection of RHC-NO_2 (200 μL, 500 μM) with 808 nm excitation, 1000 nm long-pass emission filter and exposure time of 50 ms. The full images of the mouse at different time points (0–96 h) are given in Fig. S22 (ESI†). Scale bar: 1 cm.

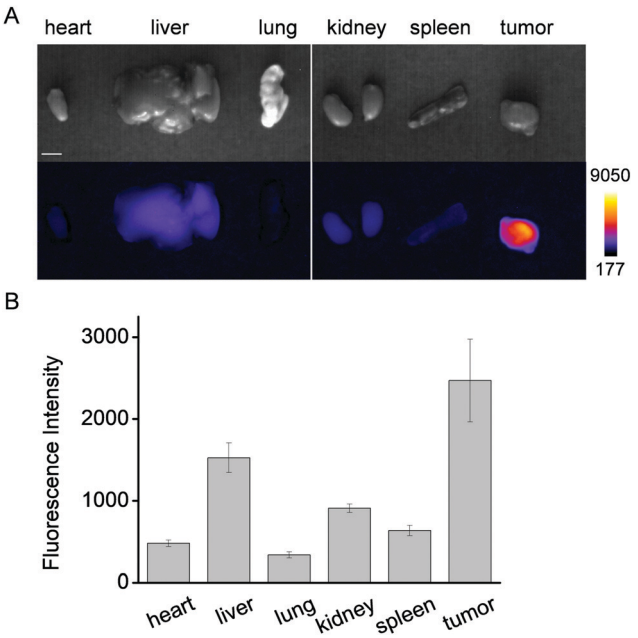

Fig. 4 *Ex vivo* biodistribution of RHC-NO_2 in A549 tumor-bearing mice after a tail vein injection of RHC-NO_2 (200 μL, 500 μM). (A) NIR-II fluorescence imaging of dissected organs and tumor after 48 h injection of RHC-NO_2 with 808 nm excitation and 1000 nm LP emission filter and exposure time of 50 ms. (B) Quantified fluorescence intensity in A549 tumor-bearing mice (n = 3). Scale bar: 5 mm.

fluorescence imaging and identification of A549 tumors. Besides, similar phenomena were observed in HeLa tumor-bearing mice (Fig. S23, ESI†), with a maximal signal detected at about 6 h. These results demonstrated the capability of RHC-NO_2 for the delineation of tumor margins in bioimaging.

Furthermore, the mice were anatomized to analyze *ex vivo* biodistribution of the probe in major organs and tumor. It was found that the NIR-II fluorescence was mostly observed in the dissected tumor after 48 h of intravenous injection of RHC-NO_2 to the A549 tumor-bearing mice (Fig. 4), with some seen in the

liver and kidney, as well. This may be explained by the fact that these two organs within the hepatobiliary and renal systems account for clearance of the probe from the body.[14] Similar results were obtained from HeLa tumor-bearing mice (Fig. S24, ESI†). The above results suggested that RHC-NO_2 could be exploited as a potential NIR fluorescent probe for cancer theranostic applications.

In summary, RHC-NO_2 has been developed as a novel NTR-activated fluorescent probe for NIR-II tumor imaging. The probe itself shows negligible fluorescence; upon reaction with NTR, however, a largely enhanced NIR-II fluorescence signal is generated with an extremely low detection limit of 5.9 ng mL^{-1}, which is about one order of magnitude lower than that (about 50 ng mL^{-1}) of the existing NIR-II fluorescence off–on probes for NTR. The high sensitivity of RHC-NO_2 makes it feasible to accurately image the tumor margins *via* detecting NTR in hypoxic tumors, and such potential has been demonstrated by *in vivo* imaging of tumor-bearing mouse models. The probe may provide a convenient way to delineate the tumor margins for theranostic research.

We are grateful to the financial support from the NSF of China (No. 21775152, 21820102007, 21922412 and 22074151).

Conflicts of interest

There are no conflicts to declare.

Notes and references

1 (*a*) H. Li, Q. Yao, W. Sun, K. Shao, Y. Lu, J. Chung, D. Kim, J. Fan, S. Long, J. Du, Y. Li, J. Wang, J. Yoon and X. Peng, *J. Am. Chem. Soc.*, 2020, **142**, 6381–6389; (*b*) R. Tian, H. Ma, S. Zhu, J. Lau, R. Ma, Y. Liu, L. Lin, S. Chandra, S. Wang, X. Zhu, H. Deng, G. Niu, M. Zhang, A. L. Antaris, K. S. Hettie, B. Yang, Y. Liang and X. Chen, *Adv. Mater.*, 2020, **32**, e1907365; (*c*) Q. Zhang, H. Zhou, H. Chen, X. Zhang, S. He, L. Ma, C. Qu, W. Fang, Y. Han, D. Wang, Y. Huang, Y. Sun, Q. Fan, Y. Chen and Z. Cheng, *Small*, 2019, **15**, e1903382.

2 (*a*) X. H. Li, X. H. Gao, W. Shi and H. M. Ma, *Chem. Rev.*, 2014, **114**, 590–659; (*b*) C. Y. Li, G. C. Chen, Y. J. Zhang, F. Wu and Q. B. Wang, *J. Am. Chem. Soc.*, 2020, **142**, 14789–14804.

3 (*a*) Z. Lei and F. Zhang, *Angew. Chem., Int. Ed.*, 2021, **60**, 16294–16308; (*b*) S. He, J. Song, J. Qu and Z. Cheng, *Chem. Soc. Rev.*, 2018, **47**, 4258–4278; (*c*) Y. Sun, F. Ding, Z. Zhou, C. Li, M. Pu, Y. Xu, Y. Zhan, X. Lu, H. Li, G. Yang, Y. Sun and P. J. Stang, *Proc. Natl. Acad. Sci. U. S. A.*, 2019, **116**, 1968–1973; (*d*) Y. Fang, J. Shang, D. Liu, W. Shi, X. Li and H. Ma, *J. Am. Chem. Soc.*, 2020, **142**, 15271–15275; (*e*) J. A. Chen, H. Pan, Z. Wang, J. Gao, J. Tan, Z. Ouyang, W. Guo and X. Gu, *Chem. Commun.*, 2020, **56**, 2731–2734; (*f*) C. Li, Y. Zhang, M. Wang, Y. Zhang, G. Chen, L. Li, D. Wu and Q. Wang, *Biomaterials*, 2014, **35**, 393–400; (*g*) J. Lin, X. Zeng, Y. Xiao, L. Tang, J. Nong, Y. Liu, H. Zhou, B. Ding, F. Xu, H. Tong, Z. Deng and X. Hong, *Chem. Sci.*, 2019, **10**, 1219–1226; (*h*) K. Shou, C. Qu, Y. Sun, H. Chen, S. Chen, L. Zhang, H. Xu, X. Hong, A. Yu and Z. Cheng, *Adv. Funct. Mater.*, 2017, **27**, 1700995; (*i*) Y. Tang, Y. Li, Z. Wang, F. Pei, X. Hu, Y. Ji, X. Li, H. Zhao, W. Hu, X. Lu, Q. Fan and W. Huang, *Chem. Commun.*, 2019, **55**, 27–30; (*j*) T. B. Ren, Z. Y. Wang, Z. Xiang, P. Lu, H. H. Lai, L. Yuan, X. B. Zhang and W. Tan, *Angew. Chem., Int. Ed.*, 2021, **60**, 800–805; (*k*) Z. Lei, C. Sun, P. Pei, S. Wang, D. Li, X. Zhang and F. Zhang, *Angew. Chem., Int. Ed.*, 2019, **58**, 8166–8171; (*l*) K. Welsher, Z. Liu, S. P. Sherlock, J. T. Robinson, Z. Chen, D. Daranciang and H. Dai, *Nat. Nanotechnol.*, 2009, **4**, 773–780; (*m*) D. J. Naczynski, M. C. Tan, M. Zevon, B. Wall, J. Kohl, A. Kulesa, S. Chen, C. M. Roth, R. E. Riman and P. V. Moghe, *Nat. Commun.*, 2013, **4**, 2199; (*n*) D. Li, S. Wang, Z. Lei, C. Sun, A. M. El-Toni, M. S. Alhoshan, Y. Fan and F. Zhang, *Anal. Chem.*, 2019, **91**, 4771–4779.

4 (*a*) N. Zhu, G. Xu, R. Wang, T. Zhu, J. Tan, X. Gu and C. Zhao, *Chem. Commun.*, 2020, **56**, 7761–7764; (*b*) Y. Li, Y. Sun, J. Li, Q. Su, W. Yuan, Y. Dai, C. Han, Q. Wang, W. Feng and F. Li, *J. Am. Chem. Soc.*, 2015, **137**, 6407–6416; (*c*) K. H. Gebremedhin, Y. Li, Q. Yao, M. Xiao, F. Gao, J. Fan, J. Du, S. Long and X. Peng, *J. Mater. Chem. B*, 2019, **7**, 408–414.

5 (*a*) S. Xu, Q. Wang, Q. Zhang, L. Zhang, L. Zuo, J. D. Jiang and H. Y. Hu, *Chem. Commun.*, 2017, **53**, 11177–11180; (*b*) X. Zhao, S. Long, M. Li, J. Cao, Y. Li, L. Guo, W. Sun, J. Du, J. Fan and X. Peng, *J. Am. Chem. Soc.*, 2020, **142**, 1510–1517; (*c*) Y. Fang, W. Shi, Y. Hu, X. Li and H. Ma, *Chem. Commun.*, 2018, **54**, 5454–5457.

6 (*a*) Z. Li, X. He, Z. Wang, R. Yang, W. Shi and H. Ma, *Biosens. Bioelectron.*, 2015, **63**, 112–116; (*b*) X. Tian, Z. Li, Y. Sun, P. Wang and H. Ma, *Anal. Chem.*, 2018, **90**, 13759–13766.

7 X. Wu, W. Shi, X. Li and H. Ma, *Acc. Chem. Res.*, 2019, **52**, 1892–1904.

8 (*a*) X. Meng, J. Zhang, Z. Sun, L. Zhou, G. Deng, S. Li, W. Li, P. Gong and L. Cai, *Theranostics*, 2018, **8**, 6025–6034; (*b*) R. Wang, J. Chen, J. Gao, J. A. Chen, G. Xu, T. Zhu, X. Gu, Z. Guo, W. H. Zhu and C. Zhao, *Chem. Sci.*, 2019, **10**, 7222–7227.

9 H. M. Ma, *Spectroscopic probes and sensing analysis*, Chemical Industry Press, Beijing, 2020.

10 (*a*) Z. Zeng, J. Ouyang, L. Sun, C. Zeng, F. Zeng and S. Wu, *Anal. Chem.*, 2020, **92**, 9257–9264; (*b*) J. Ouyang, L. Sun, Z. Zeng, C. Zeng, F. Zeng and S. Wu, *Angew. Chem., Int. Ed.*, 2020, **59**, 10111–10121.

11 B. Li, L. Lu, M. Zhao, Z. Lei and F. Zhang, *Angew. Chem., Int. Ed.*, 2018, **57**, 7483–7487.

12 (*a*) B. Zhou, Y. Li, G. Niu, M. Lan, Q. Jia and Q. Liang, *ACS Appl. Mater. Interfaces*, 2016, **8**, 29899–29905; (*b*) A. L. Antaris, H. Chen, S. Diao, Z. Ma, Z. Zhang, S. Zhu, J. Wang, A. X. Lozano, Q. Fan, L. Chew, M. Zhu, K. Cheng, X. Hong, H. Dai and Z. Cheng, *Nat. Commun.*, 2017, **8**, 15269.

13 (*a*) Q. Yu and A. A. Heikal, *J. Photochem. Photobiol., B*, 2009, **95**, 46–57; (*b*) R. S. Fletcher and G. G. Lavery, *J. Mol. Endocrinol.*, 2018, **61**, R107–R121.

14 (*a*) Y. Sun, C. Qu, H. Chen, M. He, C. Tang, K. Shou, S. Hong, M. Yang, Y. Jiang, B. Ding, Y. Xiao, L. Xing, X. Hong and Z. Cheng, *Chem. Sci.*, 2016, **7**, 6203–6207; (*b*) Y. Sun, M. Ding, X. Zeng, Y. Xiao, H. Wu, H. Zhou, B. Ding, C. Qu, W. Hou, A. Er-Bu, Y. Zhang, Z. Cheng and X. Hong, *Chem. Sci.*, 2017, **8**, 3489–3493; (*c*) A. L. Antaris, H. Chen, K. Cheng, Y. Sun, G. Hong, C. Qu, S. Diao, Z. Deng, X. Hu, B. Zhang, X. Zhang, O. K. Yaghi, Z. R. Alamparambil, X. Hong, Z. Cheng and H. Dai, *Nat. Mater.*, 2016, **15**, 235–242; (*d*) Q. Fan, K. Cheng, X. Hu, X. Ma, R. Zhang, M. Yang, X. Lu, L. Xing, W. Huang, S. S. Gambhir and Z. Cheng, *J. Am. Chem. Soc.*, 2014, **136**, 15185–15194.